



An EIGA driven coupled of electromagnetic-thermal field modeling in the induction melting process

Feng Shan¹ · Min Xia¹ · Chang-Chun Ge¹

Received: 8 March 2018 / Accepted: 31 July 2018 / Published online: 27 September 2018
© Springer-Verlag France SAS, part of Springer Nature 2018

Abstract

A crucible-free, an Electrode Induction melting Gas Atomization (EIGA) technique for induction melting of the reactive and refractory metals/alloys is developed. The impedance matching of the superalloy René95 in a conical induction has been investigated. An evaluation of the complex electromagnetic and thermal fields on the free surface of the superalloy René95 is carried out by both numerical and experimental methods under alternating currents with the output power of 120 kW and operational effective current 2 kA. The two types of coupling induction coils have been devised, tested and compared with the experimental results, revealing the impedance of four-turn induction coil with superalloy René95 releasing the electrical energy that causes the most high-temperature distribution in the surface of superalloy René95. Induction coil is also known as an “inductor” which is the core component in the melting process of nickel-based superalloy, leading to design a good induction coil to reduce the power consumption and increase the efficiency of the process. The achievements are the melting rate enhancement and a steady-state of continuous liquid metal flow producing the liquid metal streams with diameter of about 5 mm.

Keywords EIGA technique · Induction coil · Impedance matching · Superalloy René95 · Melting temperature

Introduction

There is a continuous and growing interest in developing newer electromagnetic processes to achieve high quality metallic powders, widely used in the technology driven industries like in aerospace, electronics and biomedical engineering [1, 2]. Induction heating, an electromagnetic-process, is a fast, precise, clean, energy efficient, controllable and repeatable process [3, 4]. The principles of induction heating are known for long time and are being applied to manufacturing operations since the 1930s, when the first channel-type induction furnaces were introduced for the melting operations of metals [5]. A coreless induction furnace was developed for melting, superheating, and holding which was also used to hardening

the metal engine parts in 1940s [6]. Recently, a crucible-free melting technique in combination with inert gas atomization was industrialized in the ferrous and nonferrous metals industries [7–9].

It is well-known that the ceramic inclusions can influence the material properties of high-strength powder metallurgy (P/M)-components in a negative manner [10, 11]. To avoid the “ceramic problem” in the powder production process, the crucible free techniques such as an electrode induction melting for gas atomization (EIGA) process has been applied for production of high quality alloy powders [12].

The crucible-free EIGA process is suitable for manufacturing of reactive and refractory metals/alloys powder (e.g. TiAl6V4, γ -TiAl) [13]. The parameters of an induction melting process were usually studied by numerical simulations and experimental methods [14]. Nevertheless, the electromagnetic and thermal fields are a complex system to measure it directly and accurately, and that is why many researchers preferred to do it through the numerical simulation method only. Bojarevics et al. [13] developed a numerical model of EIGA investigating the complex interaction of the electromagnetic and thermal fields on the fluid flow on a free surface. Kranjc et al. [15] used the finite element method to investigate the coupled electromagnetic and thermal physical phenomena

✉ Min Xia
xmdsg@ustb.edu.cn

✉ Chang-Chun Ge
ccge@mater.ustb.edu.cn

¹ Institute of Powder Metallurgy and Advanced Ceramics, School of Materials Science and Engineering, University of Science and Technology Beijing, NO30 Xueyuan Road, Haidian District, Beijing 100083, People’s Republic of China

in the induction heating process of steel materials. Liang Lu et al. [16] using the commercial finite element software package COMSOL-Multiphysics® analyzed the effects of an electromagnetic field, thermal and fluid flow field on the titanium wire. A few reports were focused on the melting of nickel-based superalloys and observed that, the high-frequency power of induction coil used the melting of titanium, niobium and zirconium alloys were unable to melt the nickel-based superalloy for the simple reason that different alloys had different latent heat of melting and phase change. So, to realize the induction melting of the nickel-based superalloys, it is necessary to use a design with a conical induction coil and suitable operation power parameters. The induction coil also known as an “inductor”, is an essential part of the induction melting process [17]. For a successful design of the induction coil, the inductor will depend on its number of turns in the coil, manufacturing process and maintenance which are critical to the overall efficiency of crucible-free induction melting process [18].

A novel induction melting coil is designed and developed for melting the nickel-based superalloy using the EIGA technology and it is successfully experimented the impedance matching between induction coil and superalloy, which remains the primary objective of this study. The successful coupling between the electromagnetic and thermal fields depends on the latent heat of melting and phase change of the superalloy René95, improving the thermal efficiency of the melting process and reducing the fuel consumption. It is also intended to study the consecutive melting of the nickel-based superalloy, controlling the diameter of the molten metal and achieving a steady-state and continuous liquid metal flow and the simulation results were corroborated by the experimental process.

The EIGA principle and the physical properties of material

Fig. 1 illustrates the schematic and working principle of the EIGA atomization process and it was employed in melting the nickel-based superalloy producing a fluid metal. The molten metal was introduced into a gas nozzle for atomization in presence of Argon gas, preparing the high-quality superalloy René95 P/M powders. The superalloy René95 was then immersed into a conical induction coil, and the numerical simulation and melting experiment were conducted with an output power of 120 kW at $I_{\text{eff}} = 2$ kA.

During the induction melting process, the superalloy was heated from room temperature to melting temperature. The physical properties of the melted superalloy are also dependent on many parameters and among these the heat capacity (C_p), density (ρ), viscosity (μ), diffusivity (α), conductivity (λ), surface tension (σ) and resistivity (R) were used in the melting experiments. The key physical properties of superalloy René95 listed in Table 1 [19]. The latent heat of melting

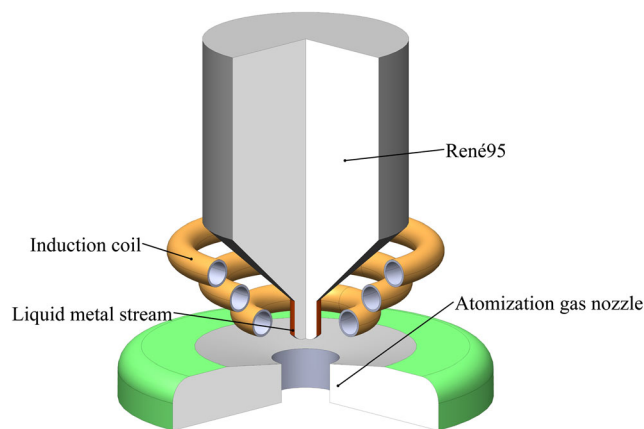


Fig. 1 Schematic diagram depicting the working principle of the EIGA atomization process

and phase change of the nickel-based superalloy René95 were measured by a differential scanning calorimetry (TGA-DSC, using the Q100 V9.9 Build, 303 model) maintaining the rate of 10 K/min constant heating and cooling in a purified argon atmosphere. The temperature of electromagnetic field was measured by high-precision infrared temperature measurement system (Marathon MM-2MH model).

The electromagnetic field is calculated by the Maxwell equations to predict the generated heat energy by induction melting. The boundary conditions of electromagnetic field are defined by the Maxwell equations which can be described as follows:

$$\nabla \times H = J + \frac{\partial D}{\partial t} \quad (1)$$

$$\nabla \times E = -\frac{\partial B}{\partial t} \quad (2)$$

$$\nabla \cdot B = 0 \quad (3)$$

$$\nabla \cdot D = \rho \quad (4)$$

Where, H refers to the magnetic field intensity (A/m), J is the current density (A/m²), D is the electric flux density (C/m²), E is the electric intensity (V/m), B is the magnetic flux density (T), ρ is the electric density (C/m) and t is the time (s). The induction coil cooling by a turbulent water flow is convective loss:

$$Q_c = \frac{dM}{dt} C_p (T_{in} - T) \quad (5)$$

where, dM/dt is the water mass flow (kg/s), C_p is the specific heat capacity of water, T_{in} is the water inlet temperature (K), T is the water outlet temperature (K), r is the radial coordinate (m) and S is the cross-section area of the cooling channel the induction coil (m²). The work flow in the module is straightforward and can be described by the following steps: defining the geometry, selecting materials and a suitable AC/DC module interface, defining the boundary, the initial conditions, and the finite element mesh, choosing a solver, and visualizing the simulation results.

Table 1 The key physical properties of superalloy René95 [19]

Physical properties	Unit	Value
Heat capacity(Cp)	J/(g·K)	0.413
Density (ρ)	g/cm ³	8.03
Viscosity (μ)	mPa·s	5.5
Diffusivity (α)	mm ² /s	4.243
Conductivity (λ)	W/(m·K)	14.010
Surface tension (σ)	N/m	1900
Resistivity (R)	Ω.cm	1.485e ⁻⁴

Results and discussion

Latent heat of melting and phase change

Latent heat of melting and the temperature at phase change were determined by TGA-DSC, and the same for the nickel-based superalloy René95 are shown in Fig. 2. The sample was heated from 20 to 1550 °C with 10 K/min in a streaming argon atmosphere (50 ml/min with the purity of 99.999%) to suppress oxidation. Fig. 2(a) shows the measurement of latent heat of melting and melting temperature are 68.6e⁺³J/g and 1420 °C, respectively. The nickel-based superalloy René95 begins to melt at 1420 °C, and the phase change and heating rate behavior are presented in Fig. 2(b). The phase transformed from solid to liquid in the temperature 1420–1550 °C. The solid superalloy René95 is completely melted at 1550 °C, and the absorbed energy was about 68.6e⁺³J/g in the melting process. It means that a superheat liquid metal can be obtained just above the temperature 1550 °C. Therefore, the most important for melting nickel-based superalloy is impedance matching with the induction coil based on the latent heat of melting and phase change of superalloy René95.

Impedance matching in induction melting

The workpiece and induction coil were reducible to an equivalent circuit model, and the nickel-based superalloy René95

and induction coil are necessary to impedance matching respectively in the melting process. Fig. 3 illustrates the geometric dimensions of the coupling design at the tip of nickel-based superalloy René95 and induction coil.

Induction melting process is a complex combination of electro-magnetic and heat transfer and there are several parameters which contribute to a coil’s effectiveness, and these are the diligent operations, the quality of raw materials used, its shape, using the appropriate and matching power source which is a critical problem, etc. Using an equivalent circuit model to design an induction coil with an effective current I_{eff} is predicted by a series RLC model of the current stimulator. In induction melting, the key issue for the superalloy René95 impedance matching is relying on the number of turns of conical induction coil as shown in Fig. 4. The superalloy René95 is matching in the conical induction coil. Hence, the melting inducting coil in Fig. 4(b) and 4(c) can be represented by Fig. 4(a) which shows effective values of inductance and resistance. The induction coils represent an inductance to the tank circuit, and the design and construction of these induction coil’s leads load can be a major factor in determining the job feasibility. The load of a circuit of induction heating power supply inverter is a typical resistor-inductor-capacitor (RLC) series circuit. The load is in the resonant circuit with an equivalent inductance and an equivalent resistance.

In a series connection, the circuits are based on resistor (R), inductor (L), and capacitor (C) in the test system. The effective current of RLC circuit may be written as:

$$I_{eff} = \frac{E}{R + jX} \tag{6}$$

where E is the induction electromotive force (V), R is the effective current equivalent resistance (Ω), and X is the effective current equivalent reactance (Ω). In a certain frequency, the melting effective current could be expressed by:

$$I_{eff} = \frac{E}{\sqrt{R^2 + X^2}} \tag{7}$$

Fig. 2 The DSC curve of nickel-based superalloy René95: **a** Latent heat of melting; **b** Phase change and heating rate

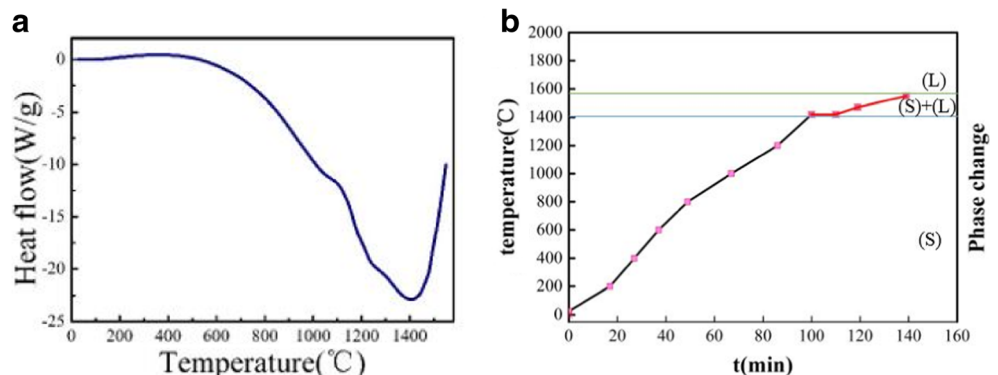
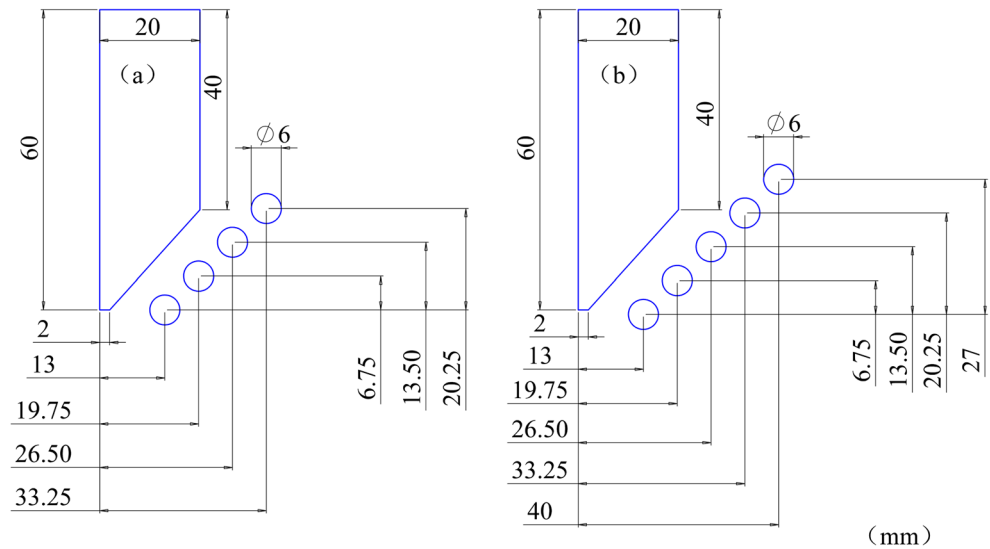


Fig. 3 The geometric dimensions of coupling design of the conical surface of nickel-based superalloy tip and induction coil: **a** Four-turn induction coil; **b** Five-turn induction coil



from the eq. (2) it can be seen, that the value of maximum current at $X = 0$ in the circuit, and the effective current equivalent reactance is represented as follows:

$$X = X_L - X_C = \omega L - \frac{1}{\omega C} \tag{8}$$

and the angular frequency, ω_0 of the circuit is described by:

$$\omega_0 = \frac{1}{\sqrt{LC}} \tag{9}$$

Skin effect and flowability of conical surface

As shown in Fig. 5, the skin effect on the conical surface of superalloy René95 is defined as the thickness of the layer, and the depth of penetration is the distance from the surface to the interior of superalloy which is to be melted. It is expressed as:

$$\delta = \frac{1}{2\pi} \sqrt{\frac{1}{\mu_r f \sigma}} \tag{10}$$

where μ_r is the relative permeability (H/m), f is the applied high-frequency (Hz), and σ is the electrical conductivity of superalloy (Ω/m). From the eq. (10), we can infer that the penetration depth, on the one hand, depends on the characteristics of the superalloy to be heated (ρ , μ) and on the other hand, it is also influenced by the frequency. The frequency dependence offers a possibility to control the heating depth and diameter of the produced molten metal stream.

Fig. 6 shows the force of gravity, normal stress and tangent stress on the fluidity of liquid metal on the conical surface. The τ_t and τ_n are the normal stress and tangent stress at the free surface, described as follows:

$$\begin{cases} \tau_t = \lim_{\Delta A \rightarrow 0} \frac{\Delta F_t}{\Delta A} \\ g = 9.8m/s^2 \\ \tau_n = \lim_{\Delta A \rightarrow 0} \frac{\Delta F_n}{\Delta A} \end{cases} \tag{11}$$

where τ_t is the tangent unit vector (N/m^2), ΔF_t is the tangent force at the free surface (N), τ_n is the normal unit vector (N/m^2), ΔF_n is the normal force at the free surface (N), and ΔA is the small area of conical free surface (m^2). The stress components for the analysis of 3D coordinates are given as matrix as follows:

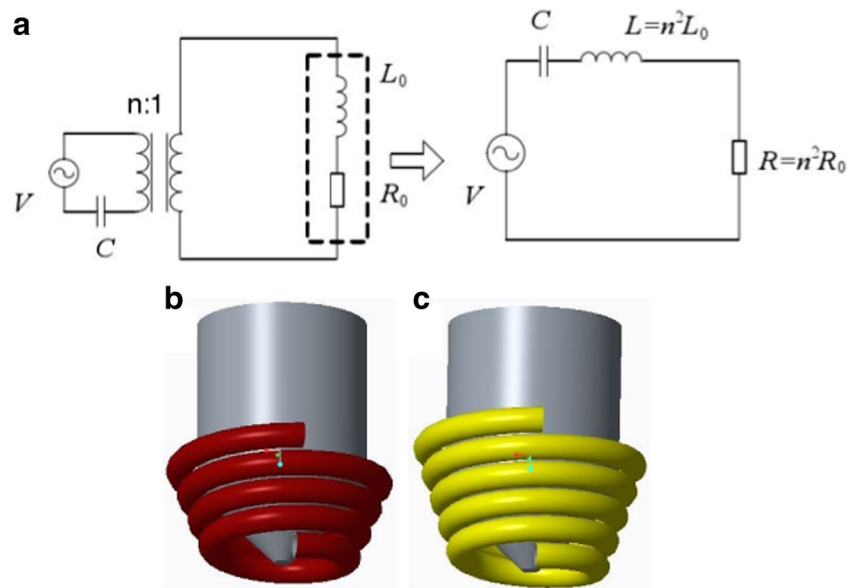
$$\tau = \begin{pmatrix} \tau_{xx} & \tau_{xy} & \tau_{xz} \\ \tau_{yx} & \tau_{yy} & \tau_{yz} \\ \tau_{zx} & \tau_{zy} & \tau_{zz} \end{pmatrix} \tag{12}$$

where τ_{xx} , τ_{yy} , τ_{zz} are the normal stress, τ_{xy} , τ_{xz} , τ_{yx} , τ_{yz} , τ_{zx} , τ_{zy} are the viscous tangent stress. The tangent stress affects the fluidity at the free surface, the viscosity and liquid metal characteristics of superalloy René95. Induction melting from solid metal to liquid metal and breaking of tangent stress to produce liquid flow as defined by the melting source from the eddy currents of induction coil. The melting energy can be expressed as follows:

$$Q = I^2 R t \tag{13}$$

where I is the eddy current (A), R is the resistance of superalloy René95 (Ω), and t is the melting time (s). However, the power supply system with an output power of 120 kW at $I_{eff} = 2$ kA, confirmed the skin effect and the flowability of conical surface on the superalloy René95.

Fig. 4 **a** Reduced circuit of the equivalent circuit; **b** Four-turn induction coil; **c** Five-turn induction coil



Four-turn induction coil

The induction coil is connected to a variable induction power supply with 120 kW at $I_{eff} = 2$ kA. The simulation results of the surface current density near a conically shaped René95 ingot immersed in a tapered four-turn induction coil is shown in Fig. 7. The current flows in a thin skin and concentrates on the conical surface of the ingot. Fig 8 shows the distribution of melting temperature on the conical surface of superalloy in electromagnetic field. Due to the maximum induction current at the surface, the surface gets heated up rapidly, and the temperature at surface layers becomes higher than the inner ones.

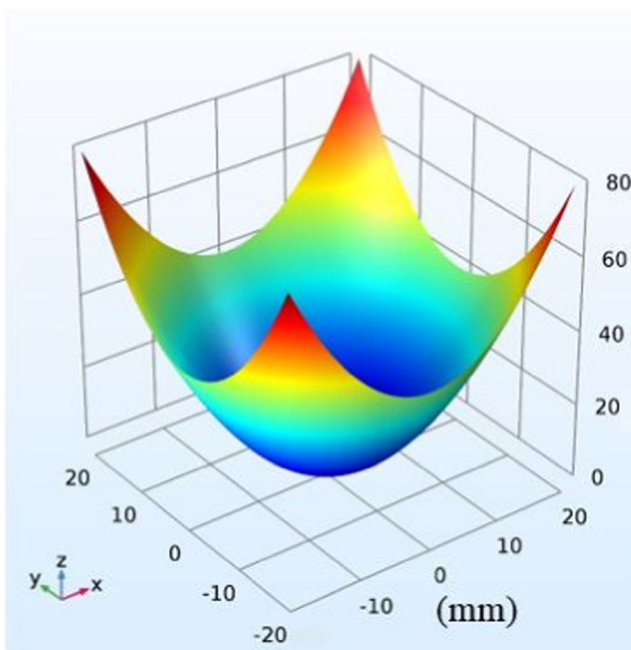


Fig. 5 The skin effect on the conical surface

The induction melting temperature (1970 °C) of the electromagnetic field is much higher than the melting point of superalloy René95 (1420 °C), so complete melting can be achieved at the thermal field as the fluid flowing at the conical of free surface. Fig. 9 shows the experimental system of superalloy René95 induction melting in the four-turn induction coil and the effective induced current with the thermal field distribution in the electrode tip. Based on the visual observation of the drip melting process, it can be assumed that the superalloy melted from the conical surface and formed a continuous and steady fluidic metal stream. The melting stage of the solid to liquid phase transformation takes only few seconds, and the actual melting temperature is 1960 °C, as measured by on-line infrared thermometer. The results closely match, the induction coil and superalloy René95 perfectly impedance matching, qualitatively and quantitatively. The superalloy René95 is fully coupled and the complex interaction of the electromagnetic and thermal fields under the output power of 120 kW at $I_{eff} = 2$ kA. However, the four-turn induction coil is an excellent system for melting the nickel-based superalloy taking the full advantage of the electromagnetic field energy.

According to the above impedance matching process, the high-frequency eddy currents derived from the

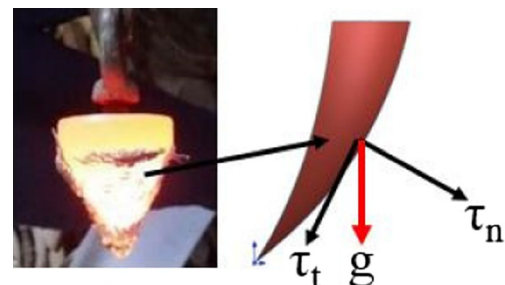


Fig. 6 Liquid metal on the conical surface

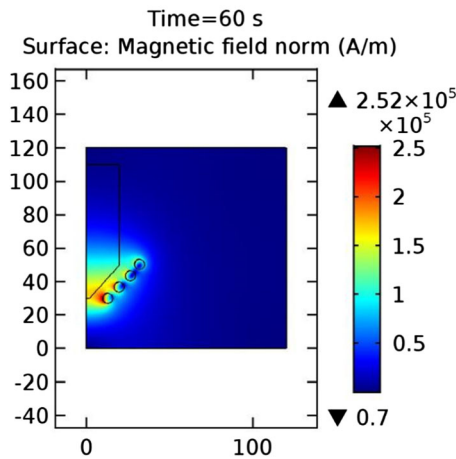


Fig. 7 Induced current density in four-turn coil

electromagnetic field generated by the alternating current power of coil. The heat is then distributed throughout the superalloy Ren95. During the melting of superalloy, a phase change occurs, and a sufficient amount of superheated energy is required for the melting process to begin and latent heat will be absorbed. A relation exists between the phase change and joule heat, where the heat balance determines the completion of melting, which produced the steady-state and a continuous flow of the liquid metal. The process based on the electromagnetic-thermal coupled equations is described by a classical heat balance equation as shown below:

$$\rho C_p \frac{\partial T}{\partial t} - \nabla(\lambda \nabla T) = Q \tag{14}$$

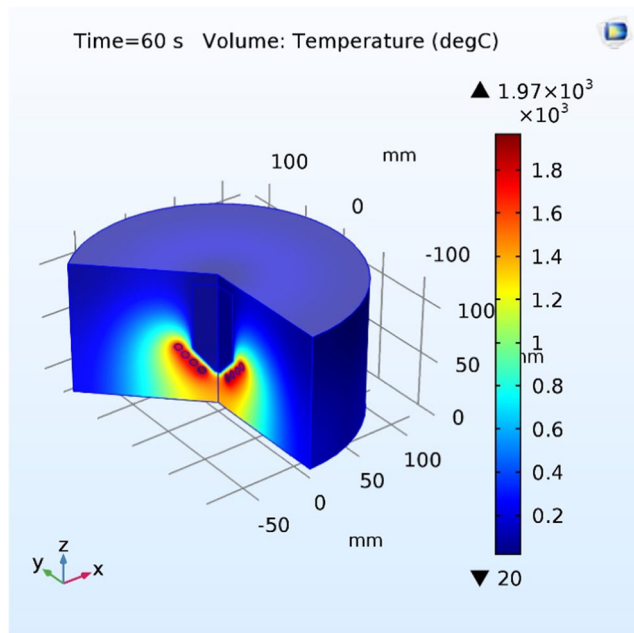


Fig. 8 Temperature distribution at the conical surface

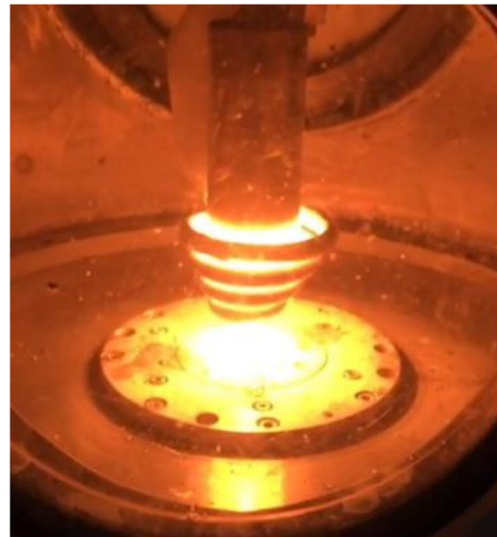


Fig. 9 Induction melting experiment with four-turn conical induction coil

$$\rho = \theta \rho_{solid} + (1-\theta) \rho_{liquid} \tag{15}$$

$$C_p = \frac{1}{\rho} (\theta \rho_{solid} C_{p.solid} + (1-\theta) \rho_{liquid} C_{p.liquid} + L \frac{\partial a_m}{\partial T}) \tag{16}$$

$$\lambda = \theta \lambda_{solid} + (1-\theta) \lambda_{liquid} \tag{17}$$

$$a_m = \frac{1}{2} \frac{(1-\theta) \rho_{solid} - \theta \rho_{liquid}}{\theta \rho_{solid} + (1-\theta) \rho_{liquid}} \tag{18}$$

$$Q = I^2 R t \tag{19}$$

Where ρ_{solid} is the density of solid phase superalloy Ren95, ρ_{liquid} is the density of liquid phase superalloy, θ is the relative content, and L is the latent heat of melting of the superalloy (J/kg), I is the eddy current (A), R is the resistance of superalloy (Ω), and t is the melting time (s).

Five-turn induction coil

As shown in Figs. 10 and 11, the simulation results of surface current density and induction melting temperature distribution on the surface of superalloy Ren95 were obtained as immersed in the five-turn induction coil. Depending on the simulation results the maximum induction melting temperature (1360 °C) is below the melting point (1420 °C) of superalloy Ren95, but the surface current density remains the same as to the results of four-turn induction coil. To validate the numerical simulation results, a similar effective (2kA) and alternating current power (120 kW) supply with the five-turn induction coil. As shown in Fig. 12, the operational experimental results under the melting parameters with 120 kW at 2 kA. In this induction melting process, based on the experimental results, two inferences can be drawn. The superalloy Ren95 is immersed into a conical induction coil,

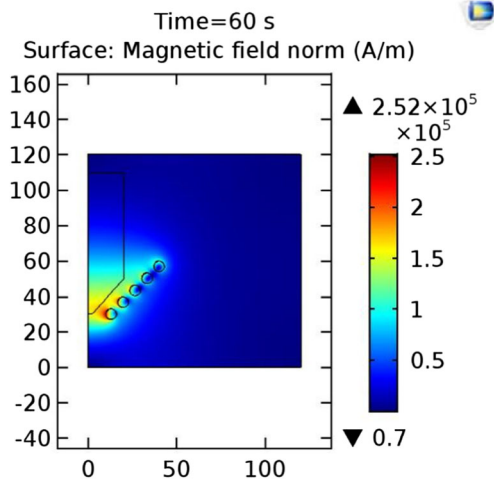


Fig. 10 Induced current density in five-turn induction coil

the surface induction temperature started to increase with an induced evolution time. The superalloy René95 cannot be melted and the distribution of the conical surface temperature is 1350 °C (measured by on-line infrared thermometer). There are some errors (about 10 °C) in the prediction, and the error was in an acceptable range. More interestingly, melting the superalloy René95 is a very complex phenomenon in the alternating current electromagnetic field. The high frequency power supply system cannot start-up in this melting experiment. This experimental result bears on the effective induction area increased and caused the induced over load in the five-turn induction coil under the melting parameters of 120 kW at 2kA. Also, the joule heat did not reach the melting point in the induction melting process. Moreover, the reason which causes the problem of impedance mismatch between the high-frequency induction coil and resistance of the superalloy René95. The joule heat is produced by the

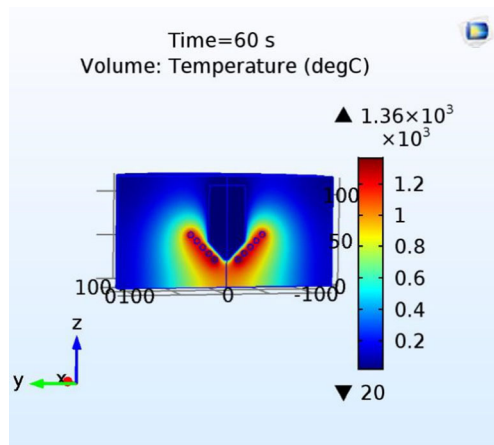


Fig. 11 Temperature distribution at conical surface



Fig. 12 Induction melting experiment with five-turn conical induction coil

eddy currents from the induction coil. The eddy currents mainly consumed at resistance of the superalloy and the resistive heat evolves in thin skin. Above the most important problems effect on the superalloy René95 impedance matching in the five-turn induction coil about the experimental melting process.

Conclusions

The superalloy René95 impedance matching in the induction coil, and its melting are investigated by numerical as well as experimental methods. The nickel-based superalloy René95 is impedance matching in the four-turn induction coil was established. The four-turn induction coil leads to a stronger electro-magnetic and thermal field when combined with the superalloy René95. The evolution of the electromagnetic and temperature field, coupling with the fluidity on the conical surface, showing an interaction with the liquid metal streams. The optimal process parameters are found to be the effective current 2 kA and at an output power of 120 kW, producing the steady-state and a continuous liquid metal flow, with a flow diameter of about 5 mm. The crucible-free technique of EIGA has been developed and applied to predict the induction melting of nickel-based superalloy and preparing high-quality powders.

Compliance with ethical standards

Conflict of interest The authors declared that they have no conflicts of interest to this work.

Publisher's Note Springer Nature remains neutral with regard to jurisdictional claims in published maps and institutional affiliations.

References

1. Franz H, Plochl L, Schimansky F-P (2008) Recent advances of titanium alloy powder production by ceramic-free inert gas atomization. *Proc Titanium*
2. Morita A, Fukui H, Tadano H, Hayashi S, Hasegawa J, Niinomi M (2000) Alloying titanium and tantalum by cold crucible levitation melting (CCLM) furnace. *Mater Sci Eng A* 280(1):208–213. [https://doi.org/10.1016/S0921-5093\(99\)00668-1](https://doi.org/10.1016/S0921-5093(99)00668-1)
3. Rudnev VI, Loveless D (2014) 12.15 - induction hardening: technology, process design, and computer modeling. In: Hashmi S, Batalha GF, Van Tyne CJ, Yilbas B (eds) *Comprehensive materials processing*. Elsevier, Oxford, pp 489–580. <https://doi.org/10.1016/B978-0-08-096532-1.01217-6>
4. Liu H, Rao J (2009) Coupled modeling of electromagnetic-thermal problem in induction heating process considering material properties. In: *Information Engineering and Computer Science. ICIECS 2009. International conference on, 2009. IEEE*, pp 1–4
5. Mühlbauer A (2008) *History of induction heating and melting*. Vulkan-Verlag, Germany
6. Atkinson M, Steel U *Improving Process Heating System Performance: A Sourcebook for Industry is a development of the BestPractices initiative under the US Department of Energy (DOE) Industrial Technologies Program (ITP) and the Industrial Heating Equipment Association (IHEA)*. The ITP and IHEA undertook this project as part of a series of Sourcebook publications on industrial utility systems. Other topics in this series include compressed air systems, pumping systems, fan systems, steam systems, and motors and drives
7. Antony LVM, Reddy RG (2003) Processes for production of high-purity metal powders. *JOM* 55(3):14–18. <https://doi.org/10.1007/s11837-003-0153-4>
8. Gerling R, Schimansky F (2004) Crucible-and ceramic-free melting and atomization of Ti-based alloys. In: *Proc. PM 2004 world congress*. European Powder Metallurgy Association, UK, pp 77–82
9. Pleier S, Goy W, Schaub B, Hohmann M, Mede M, Schumann R (2004) EIGA—an innovative production method for metal powder from reactive and refractory alloys. *PM2TEC*, MPIF, Princeton
10. Wang XF, Zhou XM, Yang J, Zou JW, Wang WX (2013) Detection and deformation mechanism of non-metallic inclusions in FG96 alloy isothermal forging disk. In: *Materials Science Forum. Trans Tech Publ*, pp 526–534
11. Ma W-b, G-q L, Hu B-f, Y-w Z, J-t L (2013) Effect of Hf on carbides of FG4096 superalloy produced by hot isostatic pressing. *Mater Sci Eng A* 587:313–319
12. Shan F, Min X, Chang-Chun G (2017) Consecutive induction melting of nickel-based superalloy in electrode induction gas atomization. *Chinese Physics B* 26(6):060201
13. Dughiero F, Baake E, Forzan M, Bojarevics V, Roy A, Pericleous K (2011) Numerical model of electrode induction melting for gas atomization. *COMPEL-The International Journal for Computation and Mathematics in Electrical and Electronic Engineering* 30(5): 1455–1466
14. Han Y, Yu E-L, Zhao T-X (2016) Three-dimensional analysis of medium-frequency induction heating of steel pipes subject to motion factor. *Int J Heat Mass Transf* 101:452–460. <https://doi.org/10.1016/j.ijheatmasstransfer.2016.05.017>
15. Kranjc M, Zupanic A, Miklavcic D, Jarm T (2010) Numerical analysis and thermographic investigation of induction heating. *Int J Heat Mass Transf* 53(17):3585–3591
16. Lu L, Zhang S, Xu J, He H, Zhao X (2017) Numerical study of titanium melting by high frequency inductive heating. *International journal of heat and mass transfer* 108 (part B):2021–2028. <https://doi.org/10.1016/j.ijheatmasstransfer.2017.01.062>
17. Wai HP, Soe S, Aung A, Win T (2008) Work coil design used in induction hardening machine
18. Fu X, Wang B, Tang X, Ji H, Zhu X (2017) Study on induction heating of workpiece before gear rolling process with different coil structures. *Appl Therm Eng* 114:1–9. <https://doi.org/10.1016/j.applthermaleng.2016.11.192>
19. Shi C, Zhong Z, Feng D (2012) *China Superalloys handbook*. China Zhijian Publishing House and Standard Press of China, Beijing, p 612